ELSEVIER

Journal of Power Sources 109 (2002) 53–57

JOURNAL OF POWER SOURCES

www.elsevier.com/locate/jpowsour

Improvement of electrochemical properties of $LiNi_{0.5}Mn_{1.5}O_4$ spinel

Xianglan Wu*, Seung Bin Kim

Department of Chemistry, Pohang University of Science and Technology, Pohang 790-784, South Korea

Received 5 September 2001; accepted 10 January 2002

Abstract

$LiNi_{0.5}Mn_{1.5}O_4$ material with a spinel structure is prepared by a sol–gel method. The material is initially fired at 850 °C and then subjected to a post-reaction annealing at 600 °C in order to minimize the nickel deficiency. The elevated firing temperature produces materials with a small surface-area which is beneficial for good capacity retention. Indeed, the spinel $LiNi_{0.5}Mn_{1.5}O_4$ not only shows a good cycle performance, but exhibits an excellent discharge capacity, i.e. 114 mAh g^{-1} at 4.66 V plateau and 127 mAh g^{-1} in total. Cyclic voltammetry and ac impedance spectroscopy are employed to characterize the reactions of lithium insertion and extraction in the $LiNi_{0.5}Mn_{1.5}O_4$ electrode. Excellent electrochemical performance and low material cost make this compound an attractive cathode for advanced lithium batteries.

Keywords: Lithium-ion battery; Lithium nickel manganese oxide; Intercalation; Impedance spectroscopy

1. Introduction

Spinel lithium manganese oxide has been studied extensively because of its high possibility of being commercialized as a cathode material for lithium-ion batteries [1–8]. Nevertheless, attempts to substitute $LiMn_2O_4$ for $LiCoO_2$ in commercial lithium-ion batteries have not been successful due to the lower specific capacity and the fast capacity fade on cycling [9–13]. To overcome these problems, partial substitution of manganese with other metals to make $LiM_xMn_{2-x}O_4$ (M = Co, Mg, Cr, Ni, Fe, Al, Ti, and Zn) has been suggested [14–18]. In the case of a small amount of substitution, the dopant reduces the initial capacity at the 4 V plateau slightly, but improves the cycle-life of the spinel greatly. By contrast, an extensive amount of substitution shows significant decrease in capacity at the 4 V plateau due to the lack of Mn^{3+} content in the spinel [1,9,19]. Recently, researchers have shown that the significant amount of capacity lost at the 4 V plateau in $LiM_xMn_{2-x}O_4$ materials reappears in a higher voltage plateau, i.e. $LiCr_{0.5}Mn_{1.5}O_4$ gives 70 mAh g^{-1} at 4.8 V [20]; $LiCu_{0.5}Mn_{1.5}O_4$ shows 25 mAh g^{-1} at 4.9 V [21,22]; $LiCoMnO_4$ exhibits 95 mAh g^{-1} at 5.0 V [23]; and $LiNi_{0.5}Mn_{1.5}O_4$ delivers 90 mAh g^{-1} at 4.7 V [24,25]. Among them, $LiCr_{0.5}Mn_{1.5}O_4$ shows a dramatic capacity fade upon cycling, whereas $LiCoMnO_4$ exhibits a drop in discharge voltage from 5.0 to 4.8 V within 36 cycles. Only $LiNi_{0.5}Mn_{1.5}O_4$ leads to acceptable stability with considerable capacity.

Spinel $LiNi_{0.5}Mn_{1.5}O_4$ prepared by the sol–gel method has been studied by two groups [24,25]. Improved capacity and cycleability were reported for material that was fired at higher temperature, though the observed capacity was still lower than the theoretical value of 149 mAh g^{-1} by about 40 mAh g^{-1}. On the other hand, the elevated firing temperature was shown to result in oxygen loss and Ni deficiency in $LiNi_{0.5}Mn_{1.5}O_4$ material, and hence cause a reduction in the length of the 4.7 V plateau. Recently, Kawai et al. [23] reported that the oxygen loss in conventional ceramic synthesis can be reduced greatly by a post-reaction annealing at 600 °C [23].

This prompted us to adopt high-temperature firing conditions and a post-reaction annealing procedure in the synthesis of $LiNi_{0.5}Mn_{1.5}O_4$ materials. Study reported here, we have prepared and characterized $LiNi_{0.5}Mn_{1.5}O_4$ that has superior capacity and stability to $LiMn_2O_4$.

2. Experimental

Spinel $LiNi_{0.5}Mn_{1.5}O_4$ was prepared from a mixture of manganese acetate, nickel nitrate and lithium hydroxide using a sol–gel method [25]. One sample was obtained by firing the dry gel at 600 °C for 24 h in air while a second

* Corresponding author. Tel.: +82-54-279-4437; fax: +82-54-279-3399.
E-mail address: wxl@postech.ac.kr (X. Wu).

0378-7753/02/$ – see front matter
PII: S0378-7753(02)00034-4

sample was prepared by firing the dry gel first at 850 °C for 12 h and then annealing at 600 °C for 24 h in air. Powder X-ray diffraction (XRD) measurements were conducted on a Rigaku RINT-1400 X-ray diffractometer using Cu Kα radiation. Scanning electron microscopy (SEM) was performed with a Hitachi S-4200 scanning electron microscope with an accelerating voltage of 8 kV. The surface-area of the material was determined by single-point nitrogen sorption using a Micromeritics ASAP 2010 surface-area analyzer. The cycling performance of the cathode materials was evaluated using coin-type cells containing a lithium metal foil anode, a separator and a cathode. The cathodes were made from mixtures of spinel $LiNi_{0.5}Mn_{1.5}O_4$ powder, acetylene black and polytetrafluoroethylene binder in a weight ratio of 80:13:7. The mixtures were rolled into thin sheets and then disc electrodes of about 0.3 cm^2 in area were cut out and attached to stainless-steel mesh current-collectors. The electrolyte was 1 M $LiPF_6$ dissolved in propylene carbonate (PC). Cells were cycled galvanostatically in a potential range of 3.5–4.9 V using an Arbin Battery Tester System.

Cyclic voltammetry and impedance spectroscopy measurements were carried out by means of an HS-3E test cell (Hohsen three electrode cell, Hohsen Co., Japan). Cyclic voltammograms were obtained at a scan rate of 0.05 mV s^{-1} over a potential range of 3.5–5.1 V versus Li/Li^+ reference electrode. Impedance experiments were carried out on $LiNi_{0.5}Mn_{1.5}O_4$ electrodes at different states-of-discharge. The data were collected in the frequency range 0.002 Hz–100 kHz with an ac voltage signal of ±15 mV.

3. Results and discussion

Powder XRD patterns for two $LiNi_{0.5}Mn_{1.5}O_4$ materials prepared by the sol–gel process are presented in Fig. 1. The observed peaks of both samples agree well with previously reported data and can be indexed to a cubic spinel structure [24,25]. It has been reported [25] that $LiNi_{0.5}Mn_{1.5}O_4$ loses oxygen and disproportionates to a spinel with a smaller Ni content and $Li_xNi_{1-x}O$ when it is heated above 650 °C. In other work [23], post-reaction annealing at 600 °C in air has been shown to prevent possible oxygen loss from the $LiCoMnO_4$ stoichiometry which was conventionally prepared by using oxidizing condition. Since $LiNi_{0.5}Mn_{1.5}O_4$ has the same spinel structure as $LiCoMnO_4$ and shows similar oxygen loss during heating, post-reaction annealing at 600 °C. was employed in the $LiNi_{0.5}Mn_{1.5}O_4$ samples prepared for the study reported here. As shown in Fig. 1, the $Li_xNi_{1-x}O$ impurity peak at the left of the (4 0 0) peak of the material fired at 850 °C is almost the same as that of the material fired at 600 °C. This is due to the post-reaction annealing which optimizes the oxygen content. The peak widths decrease, however, with increase in the firing temperature due to growth of the particle size of $LiNi_{0.5}Mn_{1.5}O_4$. These results suggest that the material fired at 850 °C has the same nickel content as the material fired at 600 °C, but has higher crystallinity. Similar results were obtained from SEM investigations. As shown in Fig. 2, the morphology of the material fired at 850 °C is very different from that of the material fired at 600 °C. The particles of

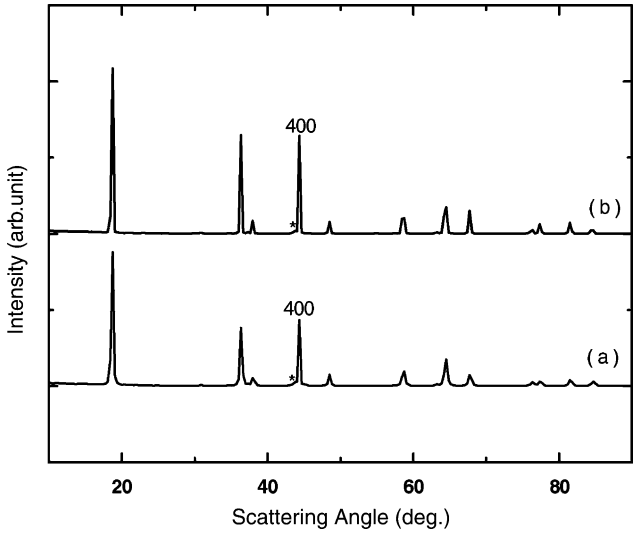

Fig. 1. Powder X-ray diffraction patterns of $LiNi_{0.5}Mn_{1.5}O_4$ samples: (a) calcined at 600 °C; (b) calcined at 850 °C and then annealed at 600 °C for 24 h.

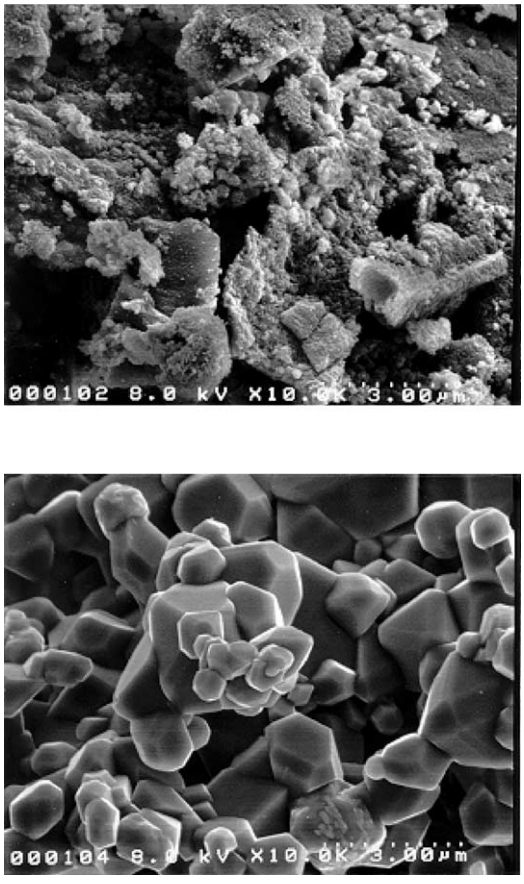

Fig. 2. Electron micrographs of $LiNi_{0.5}Mn_{1.5}O_4$ spinel calcined at 600 °C (top) and 850 °C (bottom).

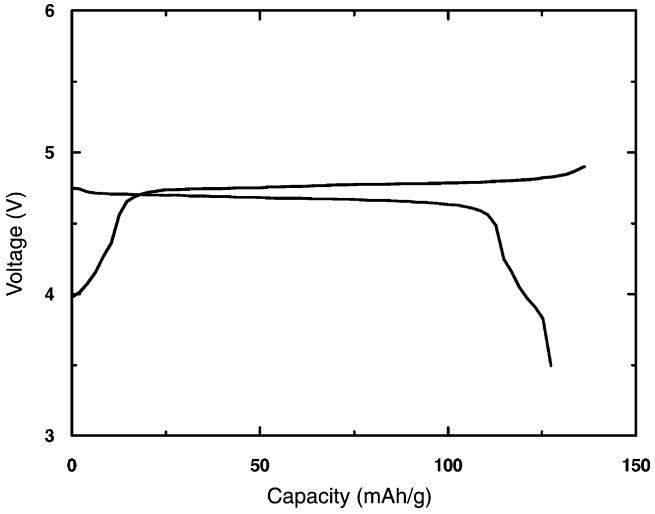

Fig. 3. First charge–discharge curves for Li/$LiNi_{0.5}Mn_{1.5}O_4$ cell in $LiPF_6$-PC. Data was collected at a current density of 0.5 mA cm^{-2} in voltage range 3.5–4.9 V.

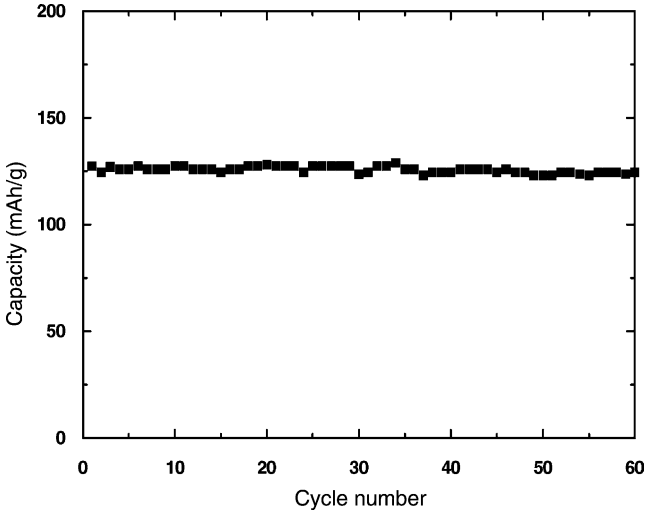

Fig. 4. Discharge capacity vs. cycle number for $LiNi_{0.5}Mn_{1.5}O_4$ cell in $LiPF_6$-PC. Data was collected at a current density of 0.5 mA cm^{-2} in voltage range 3.5–4.9 V.

the material fired at 850 °C have regular shapes with well-defined crystal faces, whereas the particles of the material fired at 600 °C are flat and loosely connected. This suggests that higher temperature produces more independent particles.

The first charge and discharge curves for a Li/$LiNi_{0.5}Mn_{1.5}O_4$ (fired at 850 °C) cell cycled between 3.5 and 4.9 V, with a current density of 0.5 mA cm^{-3}, are shown in Fig. 3. The cell delivered a capacity of 114 mAh g^{-1} at a 4.66 V plateau and 127 mAh g^{-1} in total during the initial cycle. This value is much larger than that previously reported, i.e. about 90 mAh g^{-1} at a 4.7 V plateau [24,25]. On the other hand, the first charge capacity of the cell is lower than that of previously reported data by about 20 mAh g^{-1} which indicates that there is less electrolyte decomposition. The material fired at 850 °C is found to have a surface-area of $\sim$2 m^2 g^{-1}, while the material fired at 600 °C has a surface-area of $\sim$14 m^2 g^{-1}. The dramatic reduction in surface-area is attributed to the higher temperature. These results are in good agreement with previous studies which showed that small surface-area reduces the decomposition of electrolyte and hence assists capacity retention of the cathode at both room and high-temperatures [2,9]. The result is again consistent with the XRD and SEM data which indicate that the material fired at 850 °C has higher crystallinity than material fired at 600 °C.

A plot of discharge capacity versus cycle number for a cell of the material fired at 850 °C and cycled at 0.5 mA cm^{-2} is given in Fig. 4. After 60 cycles, the total discharge capacity was still above 124 mAh g^{-1}. This value is better than those of previously obtained, i.e. 80 mAh g^{-1} on 16th cycle and 105 mAh g^{-1} on 32nd cycle, respectively [24,25]. The rate performance of the same material during discharge is presented in Fig. 5. The corresponding Li/$LiNi_{0.5}Mn_{1.5}O_4$ cells show 128, 127, 121, 108, and 100 mAh g^{-1} capacity at a current density of 0.25, 0.5, 1.0, 1.5, and 2.0 mA cm^{-2}, respectively. It is clear that the material gives similar rate performance at current densities $\leq$0.5 mA cm^{-2}.

The voltammetric behavior of a pristine $LiNi_{0.5}MniO_4$ electrode and one after 30 cycles at a scan rate of 0.05 mV s^{-1} is compared in Fig. 6. Three reversible couples appear and are related to the various phase transitions between the intercalation stages. The small peaks around 4.0 V are related to the redox couple Mn^{3+}/Mn^{4+} and its redistribution in the spinel as in the case of undoped $LiMn_2O_4$, while the large peaks at higher voltage correspond to the redox couple Ni^{2+}/Ni^{4+}. These peaks illustrate well the reversibility of this material upon de-intercalation and intercalation of lithium-ions over the potential range 3.5–5.1 V versus Li/Li^+ reference electrode. On the other hand, the negligible decrease in peak height with cycling is

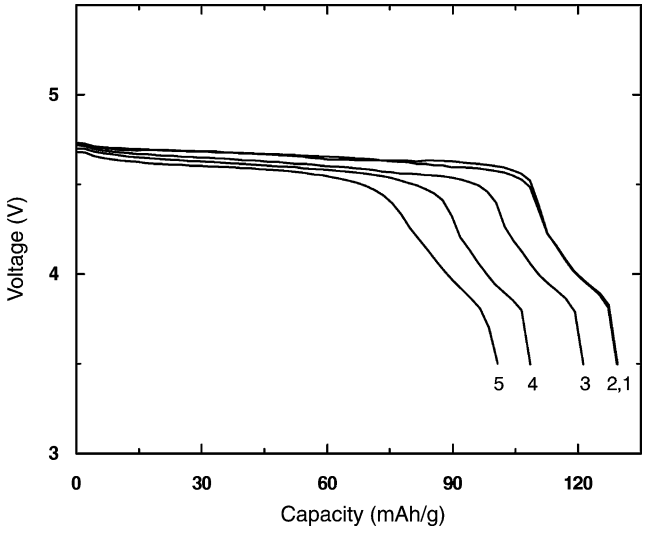

Fig. 5. Voltage vs. capacity profiles for Li/$LiNi_{0.5}Mn_{1.5}O_4$ cells as function of different discharge rates. Current densities are: (1) 0.25 mA cm^{-2}; (2) 0.5 mA cm^{-2}; (3)1.0 mA cm^{-2}; (4) 1.5 mA cm^{-2} and (5) 2.0 mA cm^{-2}.

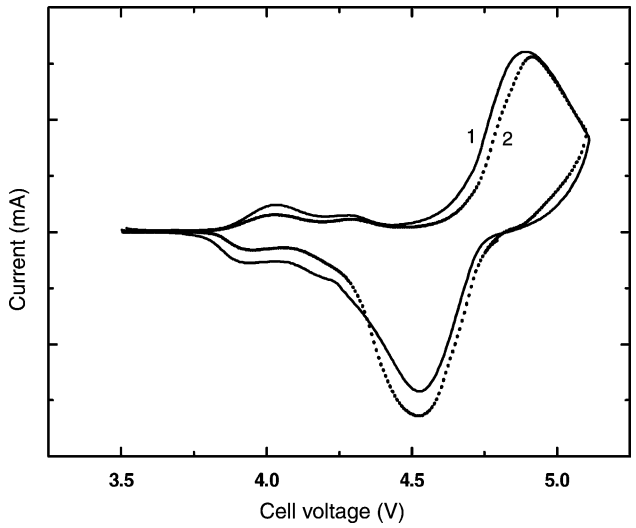

Fig. 6. Cyclic voltammograms for Li/$LiNi_{0.5}Mn_{1.5}O_4$ cells at 0.05 mV s^{-1} scan rate: (1) pristine cell; (2) after 30 cycles at 0.5 mA cm^{-2}.

in agreement with the quite small loss in capacity shown by the cycling performance profile presented in Fig. 4.

Nyquist plots obtained at different states-of-discharge are given in Fig. 7. Each plot consists of a depressed semicircle or two semicircles and a Warburg region. The depressed semicircle can be interpreted as resulting from an ionically conducting, but electronically insulating surface layer at the electrode surface and the charge-transfer process. The Warburg region at the lower frequencies is assigned to solid state diffusion of Li ions into the bulk cathode material. As has been seen for pure lithium manganese spinel [26], the size of the semicircle is strongly depended on the potential. Furthermore, the end of the semicircle is slightly distorted due to a small overlap of the charge-transfer and diffusion-controlled solution regions. The data were analyzed using

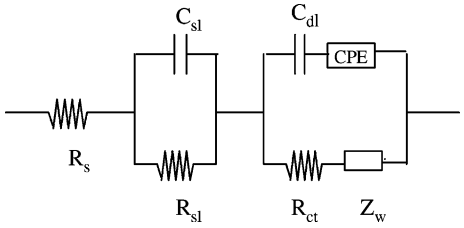

Fig. 8. Equivalent circuit for Li/$LiPF_6$-PC/$LiNi_{0.5}Mn_{1.5}O_4$ system.

the equivalent circuit shown in Fig. 8. R_{sl} represents the insertion-ion resistance, C_{sl} is the capacitance of the surface layer, R_{ct} the charge-transfer resistance, and Z_W is the Warburg impedance. To account for the depression of the semicircle, a constant phase element (CPE) in series with the double-layer capacitance (C_{dl}) was introduced into this surface-layer model.

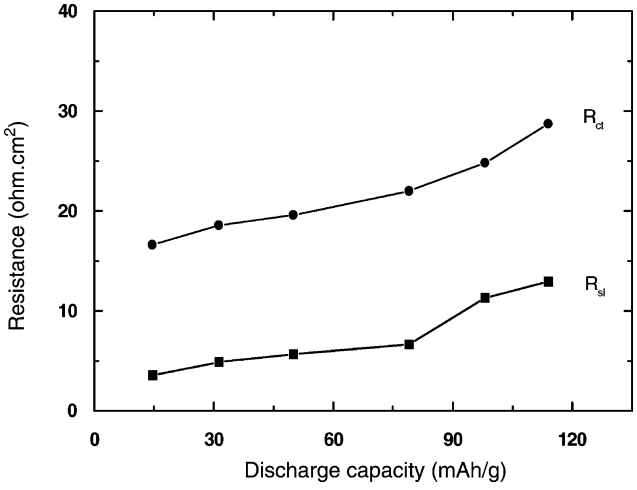

Fig. 9. Variation of charge-transfer resistance (R_{ct}) and surface-layer resistance (R_{sl}) as function of lithium insertion capacity.

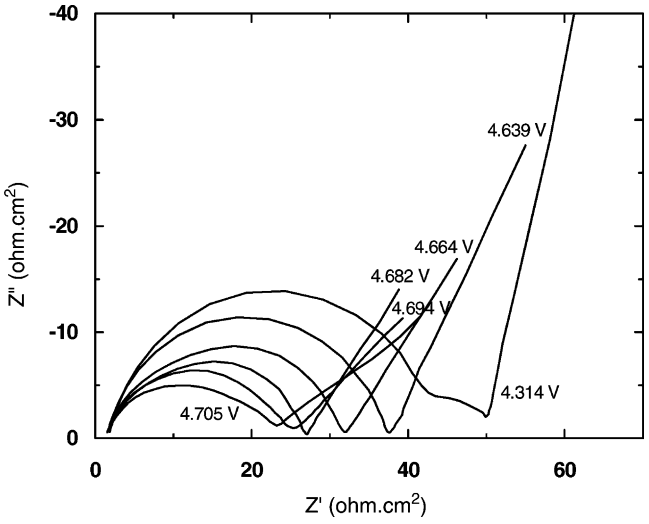

Fig. 7. Nyquist plots for $LiNi_{0.5}Mn_{1.5}O_4$ electrode at different states-of-discharge.

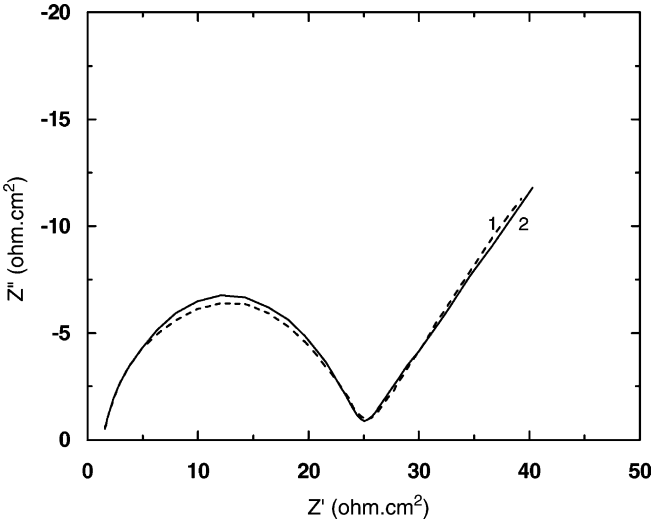

Fig. 10. Nyquist plots for $LiNi_{0.5}Mn_{1.5}O_4$ electrode obtained at 4.705 V after (1) first cycle; (2) 30th cycle.

The behavior of both the charge-transfer and surface-layer resistance as a function of lithium insertion capacity is presented in Fig. 9. The observed increase in R_{sl} is due to the slow growth of the passive film as a function of time and voltage. The higher the potential, and the more the lithium is depleted, so the charge-transfer resistance becomes monotonically smaller. Similar results have been obtained by Zhang et al. [10] in an impedance analysis of $LiCr_{0.1}Mn_{1.9}O_4$. It was shown that both R_{sl} and R_{ct} depended on the state-of-charge at the 100th cycle. Impedance spectra measured at the same voltage (4.705 V versus Li/Li^+) for a lithium depleated electrode after 1 and 30 cycles are given in Fig. 10. It is seen that the spectrum is virtually unchanged with cycling. This indicates that the electrode maintains good stability.

4. Conclusions

Spinel $LiNi_{0.5}Mn_{1.5}O_4$ is prepared by the sol–gel method. The material is fired at 850 °C and subjected to post-reaction annealing at 600 °C to reduce oxygen loss and improve Ni content. The procedure endows sample with higher crystallinity and hence reduces electrolyte decomposition. The material delivers a capacity of 127 mAh g^{-1} on the first cycle and sustains a value of 124 mAh g^{-1} even after 60 cycles. Impedance spectra are characterized by a surface film loop in the high-frequency region, a charge-transfer loop in the middle-frequency region and a capacitive loop or distorted Warburg tail in the low-frequency region.

References

[1] K. Amine, H. Tukamoto, H. Yasuda, Y. Fujita, J. Electrochem. Soc. 143 (1996) 1607.
[2] Y. Xia, Y. Zhou, M. Yoshio, J. Electrochem. Soc. 144 (1997) 2593.
[3] M. Hosoya, H. Ikuta, M. Wakihara, Solid State Ionics 111 (1998) 153.
[4] D. Peramunage, K.M. Abraham, J. Electrochem. Soc. 145 (1998) 1131.
[5] X. Qiu, X. Sun, W. Shen, N. Chen, Solid State Ionics 93 (1997) 335.
[6] H. Huang, C.H. Chen, R.C. Perego, E.M. Kelder, L. Chen, J. Schoonman, W.J. Weydanz, D.W. Nielsen, Solid State Ionics 127 (2000) 31.
[7] M.Y. Saïdi, J. Barker, R. Koksbang, Electrochim. Acta 41 (1996) 199.
[8] G.G. Amatucci, A. Blyr, C. Sigala, P. Alfonse, J.M. Tarascon, Solid State Ionics 104 (1997) 13.
[9] P. Arora, B.N. Popov, R.E. White, J. Electrochem. Soc. 145 (1998) 807.
[10] D. Zhang, B.N. Popov, R.E. White, J. Power Sources 76 (1998) 81.
[11] G.X. Wang, D.H. Bradhurst, H.K. Liu, S.X. Dou, Solid State lonics 120 (1999) 95.
[12] C. Tsang, A. Manthiram, Solid State lonics 89 (1996) 305.
[13] L. Hernán, J. Morales, L. Sánchez, J. Santos, Solid State Ionics 104 (1997) 205.
[14] A.D. Robertson, S.H. Lu, W.F. Averill, W.F. Howard, J. Electrochem. Soc. 144 (1997) 3500.
[15] D. Song, H. Ikuta, T. Uchida, M. Wakihara, Solid State lonics 117 (1999) 151.
[16] F. Le cras, D. Bloch, M. Anne, P. Strobel, Solid State lonics 89 (1996) 203.
[17] L. Hernan, J. Morales, L. Sanchez, J. Santos, Solid State lonics 118 (1999) 179.
[18] J.M. Tarascon, E. Wang, F.K. Shokoohi, W.R. Mckinnon, S. Colson, J. Electrochem. Soc. 138 (1991) 2859.
[19] J.M. Amarilla, J.L.M. de Vidales, R.M. Rojas, Solid State Ionics 127 (2000) 73.
[20] C. Sigala, D. Guyomard, A. Verbaere, Y. Piffard, M. Tournoux, Solid State Ionics 81 (1995) 167.
[21] Y.E. Eli, W.F. Howard Jr., J. Electrochem. Soc. 144 (1997) L205.
[22] Y.E. Eli, W.F. Howard, S.H. Lu, S. Mukerjee, J. Mcbreen, J.T. Vaughey, M.M. Thackeray, J. Electrochem. Soc. 145 (1998) 1238.
[23] H. Kawai, M. Nagata, H. Tukamoto, A.R. West, Electrochem. Solid State Lett. 1 (1998) 212.
[24] K. Amine, H. Tukamoto, H. Yasuda, Y. Fujita, J. Power Sources 68 (1997) 604.
[25] Q. Zhong, A. Bonakdarpour, M. Zhang, Y. Gao, J.R. Dahn, J. Electrochem. Soc. 144 (1997) 205.
[26] D. Aurbach, M.D. Levi, E. Levi, H. Teller, B. Markovsky, G. Salitra, U. Heider, L. Heider, J. Electrochem. Soc. 145 (1998) 3024.